Complex characterization of power LEDs: simultaneous measurement of photometric/radiometric and thermal properties

G. Farkas[1], A. Poppe[1, 2], J. Schanda[3], K. Muray[4],

[1] MicReD Ltd., Hungary, [2] Budapest University of Technology & Economics, Hungary
[3] University of Veszprém, Hungary, [4] Inphora Inc., USA,

1 Introduction

In case of power LEDs used as light sources, thermal issues are important. Although light conversion efficiency of these devices is rather high, 65-70% of the supplied electrical power heats up the LED that results in junction temperature rise of 25-50 ^{o}C, depending on the thermal resistance of the device and its enclosure. Thus, besides reaching high efficiency and meeting photometric targets, the proper thermal management of the power LED devices is gaining importance. Since the power of LEDs used in lighting is 1 to 10 Watts, severe overheating problems may occur and like in case of any semiconductor device, this overheating may destroy the device which otherwise would have an infinite lifetime. In other words, the junction-to-case / junction-to-ambient thermal resistance (or in general, thermal impedance) must be kept at minimum in order to minimize the temperature rise at the light emitting region of a LED device, ensuring its expected lifetime and reliability. In addition to that, the good thermal management is also a key factor in avoiding thermally induced variation of the photometric / colorimetric properties of power LEDs, such as variation of relative light output or the spectrum (Figure 1).

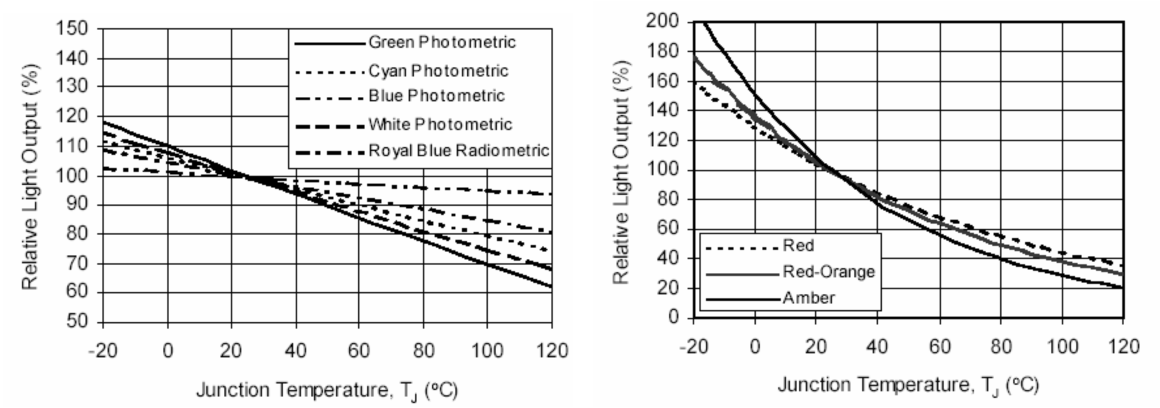

a)

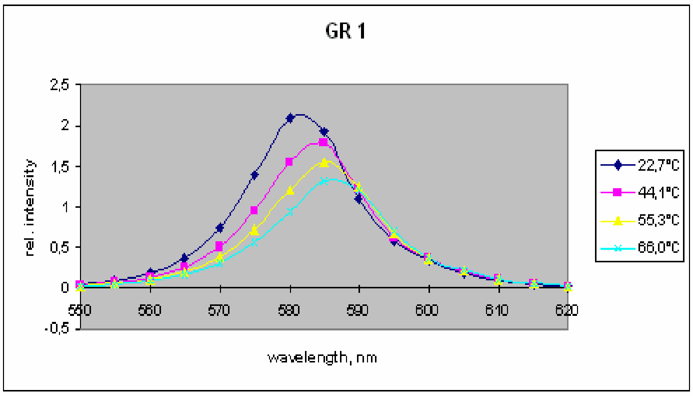

b)

Figure 1: Temperature dependence of photometric/radiometric parameters of LEDs: a) Variation of relative light output of power LEDs (source: www.lumileds.com), b) variation of the relative spectral distribution of a green LED

The need for a combined photometric/radiometric/thermal characterization of LED devices originates also from the standard device characterization procedures of the semiconductor industry. In case of semiconductor devices, besides their electrical characteristics thermal parameters such as junction-to-case thermal resistance are also important. The same applies for the light emitting diodes. In case of conventional semiconductor devices the total electrical power supplied to the device is dissipated in form of heat, while in case of LEDs about 30-35% of the power is converted to light. Thus, thermal characterization of LEDs cannot be completed properly without knowing the energy flux emitted as light (radiometric flux), that is why radiometric characterization of a LED device is a pre-requisite for its thermal characterization as a semiconductor device.

In case of photometry/radiometry of LEDs the stabilized temperature of the PN junction is required in order to avoid variations shown in Figure 1: the measurement takes place in thermal equilibrium. Upon completing the measurement, when switching off the LED, its cooling transient starts which can be recorded by thermal transient testers [1] used for thermal characterization. As Figure 2 suggests, they can be carried out in series. The photometric/radiometric measurements are carried out after a heating period, in thermal and electrical stead-state and then the thermal characterization usually based on a captured cooling transient inherently complement one another.

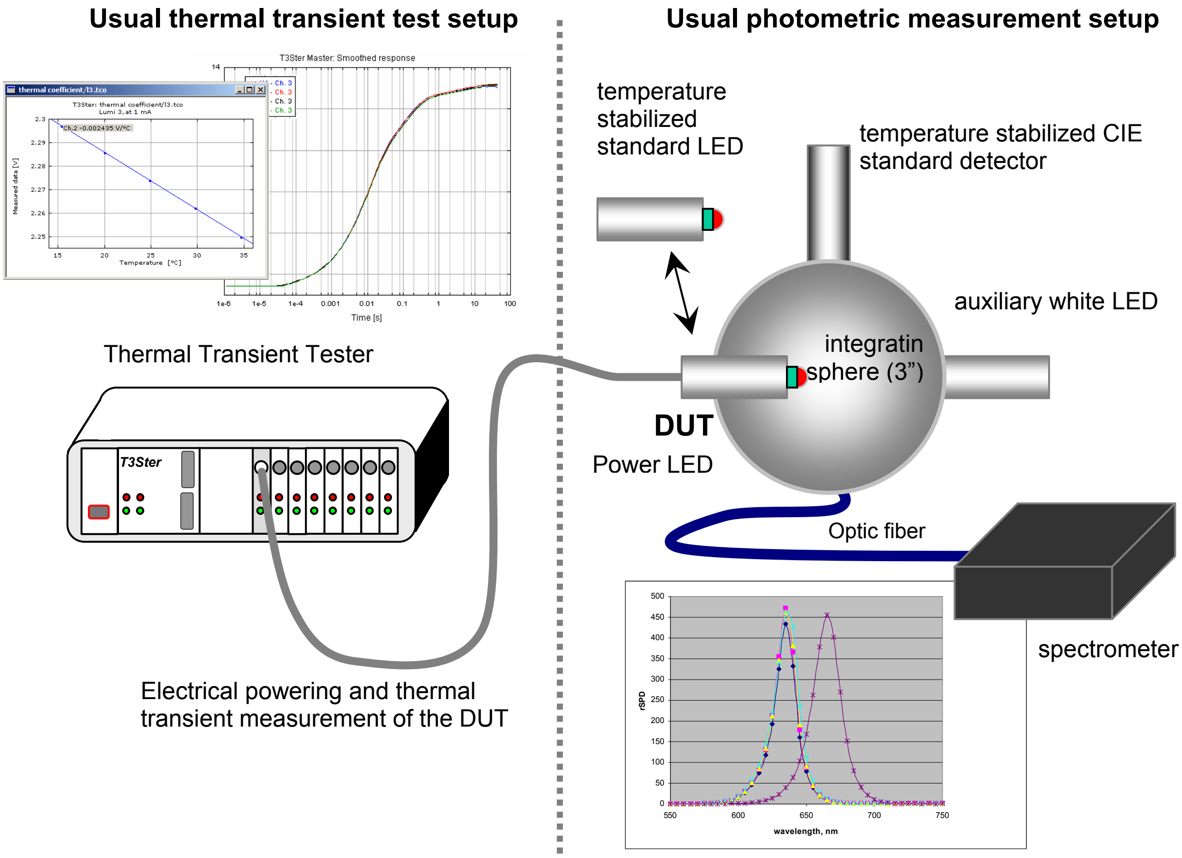

Figure 2: Combined thermal and photometric/radiometric measurement setup for the characterization of power LEDs

2 Thermal transient characterization

In many cases packaging of semiconductor devices is characterized by a single, lumped steady-state value like *junction-to-case* or *junction-to-ambient* thermal resistance. There are well established industrial standards [2] to measure these steady-state parameters. Any increase in the lumped steady-state thermal resistance of a packaged device is a good indicator of packaging or assembly problems, but more information is needed if one tries to locate the source of problem in the junction-to-ambient heat-conduction path. Thermal transient measurements yield all data of a device package. Typically after having applied a power step at the junction its temperature transient is recorded. Such a step response can be either a *heating curve* or a *cooling curve* – see

Figure 3. If the transient curve is normalized to +1W power step, it is also referred to as *thermal impedance curve* or *thermal unit-step response*. When it is known, structural details of its junction-to-ambient heat-conduction path can be identified by sophisticated procedures [3]. The method used in our work is called the NID method – that is *network identification by deconvolution*. Thus, the ultimate result of the evaluation procedure is a detailed thermal RC ladder network model (with about 150-200 stages) such as shown in Figure 4. This ladder is called Cauer-type model in electronics and its elements have direct physical meaning.

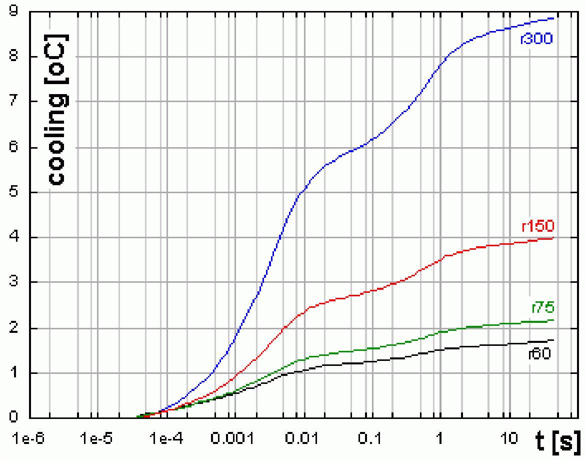

Figure 3: Cooling curves of a red 1W power LED at different bias current levels (300mA, 150mA, 75mA, 60mA)

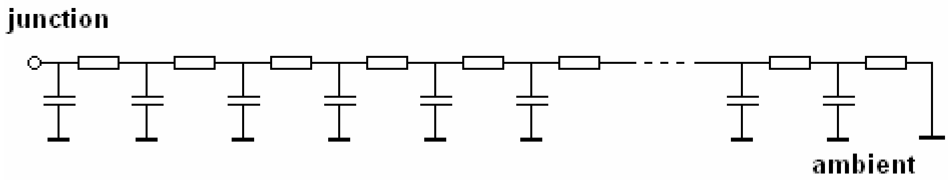

Figure 4: Cauer-type RC ladder network model of a thermal impedance in the Cauer canonic form

The NID evaluation method uses deconvolution which gives usable results only if the thermal transients are very accurate and noise free. The system we use carries out the transient measurement in real-time using a very high sampling rate (100…1000 samples in an octave of time) with a temperature measurement accuracy in the order of magnitude of 0.01..0.05°C, depending on the temperature dependence of the forward voltage of the PN junction.

2.1 Structure functions

The Cauer-type RC ladder model is the ultimate results of the evaluation of the measured thermal transients. But these model networks are of a few hundred stages and hard to handle. In order to allow a straightforward interpretation, the *structure functions* have been introduced by Székely [3], [4], [5]. The concept of structure functions is explained by. We define the cumulative thermal resistance and the cumulative thermal capacitance along the heat-flow path as the sum of the thermal resistance and thermal capacitance element values of the Cauer-type model network:

$$R_{\Sigma n} = \sum_{i=1}^{n} R_i \,, \quad C_{\Sigma n} = \sum_{i=1}^{n} C_i \tag{1}$$

Using the cumulative values we can construct the $C_\Sigma(R_\Sigma)$ function which is called the cumulative or integral structure function. Since the cumulative thermal capacitance spans many orders of magnitude and tends to infinity at the ambient (universe), in graphical representation usually its logarithm is plotted. Sudden changes in the integral structure function correspond to sudden material or geometric changes in the heat-flow path, thus, different structural elements of the heat-flow path can be identified between the inflection points of the integral structure function. In order to easily locate these boundaries we also define the differential structure function:

$$K(R_\Sigma) = \frac{dC_\Sigma}{dR_\Sigma} \tag{2}$$

It can be easily proven, that the value of K is proportional to the square of the cross-sectional area of the heat-flow path through the c volumetric specific capacitance and l thermal conductivity of the material. For the material slice of dx width and A cross-sectional area (Figure 6) one can express its thermal capacitance: $dC_\Sigma = c\ dV = cA\ dx$ and thermal resistance ?$dR_\Sigma = (1/l)\ (dx/A)$ yielding

$$K(R_\Sigma) = \frac{dC_\Sigma}{dR_\Sigma} = \frac{cAdx}{dx / lA} = c l A^2 \quad . \tag{3}$$

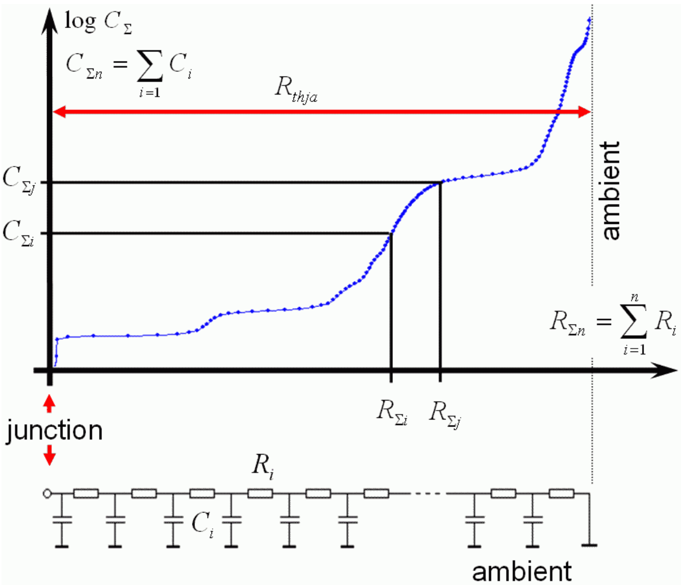

Figure 5: The cumulative or integral structure function: the cumulative thermal capacitance vs. cumulative thermal resistance plot

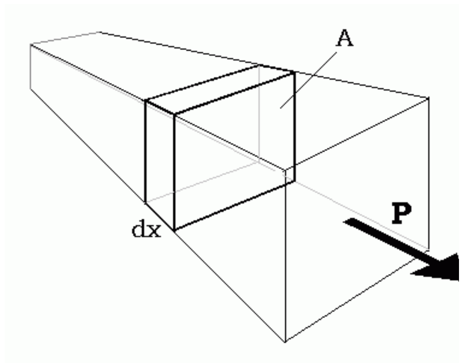

Figure 6: For the interpretation of the differential structure function: heat-flow in a homogeneous rod

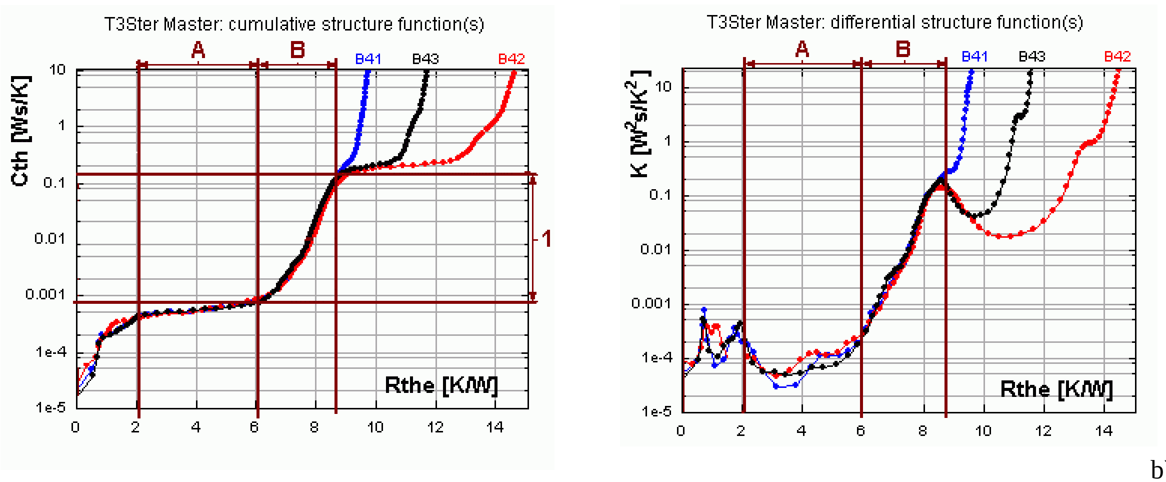

a) b)

Figure 7: Structure functions obtained for 3 power LEDs from the same manufacturing lot: a) integral structure functions, b) differential structure functions

Structure functions are thermal capacitance / thermal resistance maps of the junction-to-ambient heat-conduction path. If the heat-flow is essentially one-dimensional – that is there are no concurrent, parallel paths – there is a one-to-one correspondence between the structure functions and the physical heat-conduction structure, this way structure functions are direct models of the heat-flow path and are ideal means for a *non-destructive structure analysis*. This way e.g. the die attach – which is one of the most critical elements of the heat-flow path in semiconductor devices – can be qualified.

Since the structure functions characterize solely the junction-to-ambient heat-flow path, in principle they are independent from the power level applied during the measurement of the thermal transient, thus, they are inherently normalized.

Figure 7 presents structure functions obtained for three different power LEDs from the same manufacturing lot. As it can be seen, partial thermal resistances can be well identified from the differential structure functions (distance between adjacent peaks) while thermal capacitance values can be read from the integral ones. In Figure 7 structure functions of all devices coincide well for the heat-flow path portions inside the package. The fixing force was different for the three samples, so the case-to-ambient section varies. This is not disturbing and helps identify the junction-to-case section of the structure functions.

2.2 Measurement results

We carried out two kinds of thermal transient measurements:

- we investigated 1W power LEDs from the same manufacturing batch at the same power level (see the calculated structure functions in Figure 7) and
- We investigated a single 1W power LED device at different electrical power levels (see the thermal transients in Figure 3).

In the second case we derived the structure functions again and we found, that the structure functions varied as the supplied electrical power was increased. (The applied bias current was 60, 75, 150 and 300 mA.)

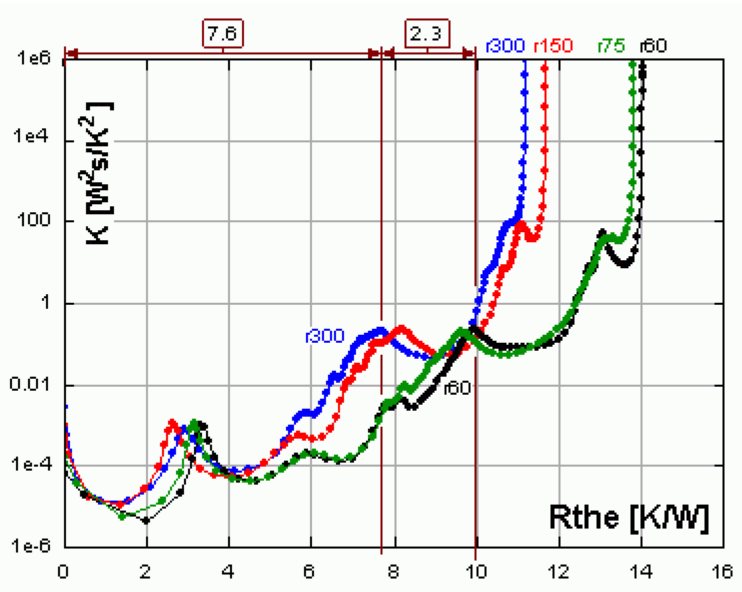

Figure 8: Differential structure functions obtained for a 1W red power LED at bias levels of 60, 70, 150 and 300 mA

Since the device structure was not changed, only the powering, we tried to find a proper explanation of the shrinking of structure function with increasing electrical input power.

3 Results of combined ThErmal and RAdiometric measurements of a power LED

In search for explanation of electrical input power dependence of the structure functions, we created a combined thermal and photometric/radiometric measurement setup as shown in Figure 2. The steady-state powering of the measured LED was provided by a high speed, high resolution thermal transient tester equipment[1]. Since we had no radiometric detector having the required accuracy in the spectrum range of the tested LED, the measurement of the emitted radiometric flux was traced back to the measurement of the Φ luminous flux of our LED as

$$\Phi = \Phi_n \cdot (Y_x / Y_n) \cdot (Y_{hn} / Y_{hx}) \qquad (4)$$

When the standard LED of known Φ_n luminous flux was in the integrating sphere we obtained Y_n detector current. The detector current obtained with the device under test (DUT) was Y_x. The package and the fixture of the standard LED and the DUT differs, this was corrected using an auxiliary white LED. When the auxiliary LED was lit we measured Y_{hx} and Y_{hn} detector currents, respectively, with the DUT and the standard LED in the sphere. The radiometric flux of the device under test was calculated as

$$\Phi = 683 \int_{380nm}^{780nm} S_l V(l) \mathrm{d}l = K \cdot 683 \cdot \sum_{550nm}^{750nm} S_{\mathrm{rel}}(l) \cdot V(l) \cdot \Delta l \qquad (5)$$

where S_λ is the absolute *radiometric* flux to be determined, $V(\lambda)$ is the CIE 1924 visibility function, $S_{\mathrm{rel}}(\lambda)$ is the relative spectral distribution of the measured LED (Figure 9), $\Delta\lambda$ is the sampling bandwidth of the calculation and 683 lm/W is the conversion constant between the luminous and radiometric flux. Summation was restricted to the 550 nm to 750 nm wavelength interval where considerable emission occurred. From the calculated K values P_{opt} has been identified for all powering levels, see Table 1.

I_F [mA]	60	75	150	300
I_{det} [μA]	16.38	20.03	38.15	72.71
Φ_x flux [lm]	7.77	9.50	18.09	34.48
P_{opt} [mW]	45.1	54.5	106	205
P_{el} [mW]	122	156	342	790
η	0.37	0.35	0.31	0.26

Table 1: Results of the photometric measurement of a 1W red power LED

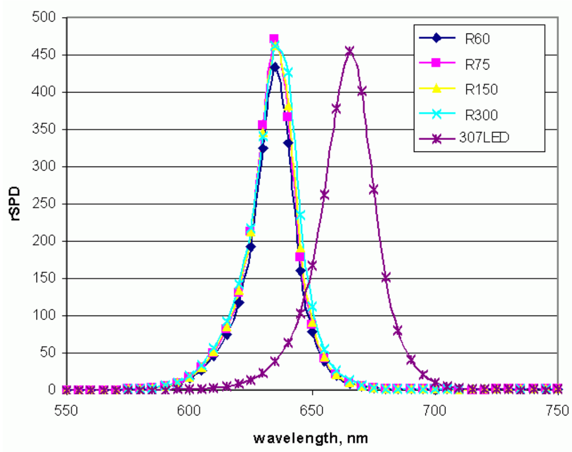

Figure 9: Relative spectral power distribution of the reference LED; and the measured 1W red power LED at different powering

Table 1 shows the dependence of the η light emission efficiency on current level. Other measurements proved that with growing forward current η increases at until approximately 5 mA and diminishes afterwards.

4 Modeling

For explaining the effects experienced in the measurements we have to follow the electrons on their adventurous way through the packaged device. They pass through gold wires, semiconductor regions of different bandgap and interface surfaces between metals and semiconductors. They interact with fields and particles in the crystals causing various energy transports. Physicists like to put labels on this phenomena as "ambipolar diffusion", "Joule heat on serial resistance", "non-radiative recombination" etc. There is only one layer of a few atoms thickness in the packaged device, where the conversion of the electric energy to light occurs. The neighbourhood of this active layer is the PN junction.

It helps understanding complex effects creating models of different levels of them. Below we suggest a semi-empirical model where electric phenomena are lumped in two elements only. The bulk of the events going on in the junction is concentrated in an „ideal diode" having typical exponential characteristics. Secondary effects in the junction and everything farther from it is treated as „serial resistance" as these interactions produce heat only (Figure 11).

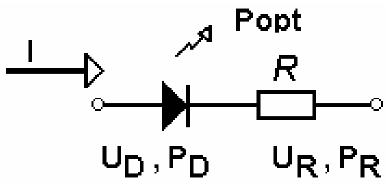

Figure 10: Simple LED model

In this model all energy not emitted as light is assumed to heat the device:

$$P_{heat} = P_{el} - P_{opt} \ , \tag{6}$$

The junction emits P_{opt} optical power. The heating power defined by Eq. (6) is distributed between the junction and the serial resistance:

$$P_{heat} = P_D - P_{opt} + P_R \tag{7}$$

where P_D denotes the electrical power dissipated on the junction and P_R is the power dissipated on the serial resistance.

The model parameters can be easily identified, combined measurements for getting P_{opt} were shown in the previous section, the serial resistance of the device can be measured electrically in the same setup..

Also, one may consider the fact that part of the emitted optical power is absorbed in the LED and contributes to its heating. A model considering all these possible effects is shown in Figure 11.

Having introduced different power values, we cannot avoid defining two different thermal resistance values, too. On one hand *the effective thermal resistance* reads as

$$R_{the} \ = \Delta T / \ P_{el} \tag{8}$$

that equals to the thermal resistance defined for conventional electrical components. On the other hand, the *real or internal thermal resistance* of a LED can be defined as

$$R_{thr} \ = \Delta T / \ P_{heat} = \Delta T / \ (P_{el} - P_{opt}) \tag{9}$$

This R_{thr} thermal resistance value can be used for characterizing package quality, not influenced by the actual type (color, etc.) of the packaged LED. We have to note, that the structure functions shown in Figure 8 were scaled in R_{the}. We may rescale these figures to R_{thr} , for package data sheets etc.

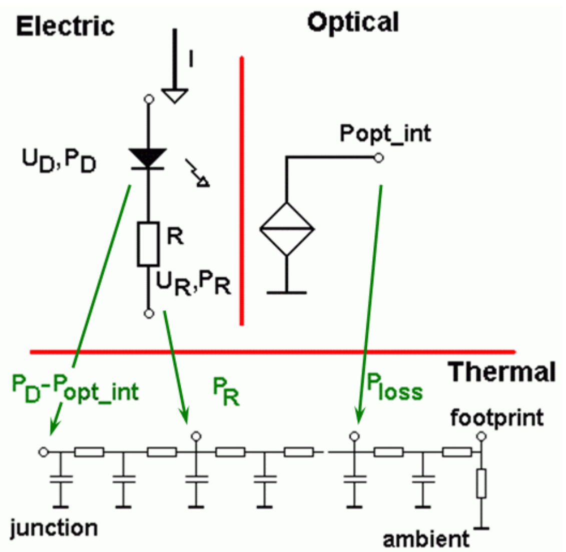

Figure 11: General mixed model of a power LED

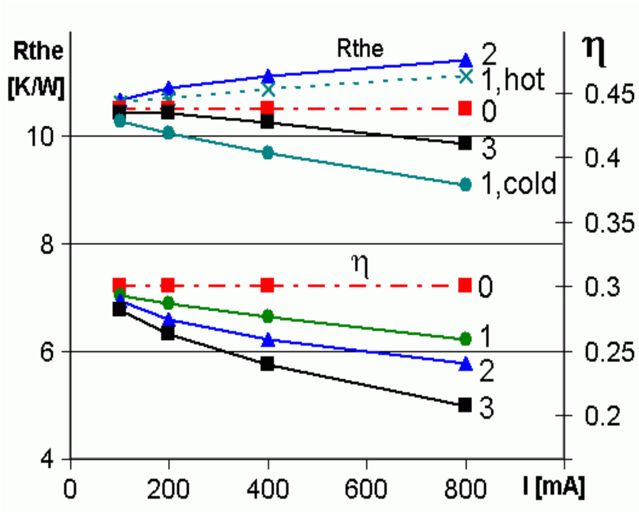

Figure 12: Efficiency and thermal resistance values, comparison of four models

4.1 Analytical models of different complexity

We created several models for describing LED devices. First we made *analytical* models expressed in a closed formula for easy handling of the problem. Here all thermal effects were concentrated into a single resistor. In some models we also assumed that the resistor is very near to the ideal diode section, or, on the contrary, it is at a geometrically far location.

Regarding the P_{opt} emitted power we modeled LEDs with two basic assumptions:

- it is proportional to the P_D electrical power of the PN junction only, or
- it is proportional to the I_F forward current of the diode

Also, in both cases we created models where

- The effect of the serial resistance was neglected
- The effect of the serial resistance was considered

We hoped that comparing simulated results of different model levels to measured data we can identify the physical causes of shrinking and expanding thermal resistance curves.

Serial resistance	neglected	considered
P_{opt} proportional to		
P_D	level 0	level 1
I_F	level 2	level 3

Table 2: Different model levels used for describing power LEDs

<u>In the simplest, *level 0* model</u> we suppose that our device has a constant h_O efficiency and currents are relatively low, the electric loss of P_R can be neglected. The LED emits $P_{opt} = h_O \cdot P_D$ optical power regardless of the power level. If the package has R_{thr} thermal resistance we measure

$$R_{the} = R_{thr} \cdot P_{heat} / P_D = (1-h_O) \cdot R_{thr} \qquad (10)$$

where η_O denotes the efficiency of the LED assumed to be a constant value for this model.

<u>In *model level 1*</u> we take electrical losses into account saying $P_{el} = P_D + P_R$. Now we experience an h_1 actual efficiency lower than h_O above at high current levels:

$$\eta_1 = P_{opt} / P_{el} = \eta_O \cdot P_D / (P_D + P_R) \qquad (11)$$

In [6] we have shown that the location of electric losses in the physical structure influences the thermal behavior. The extreme positions of the serial resistance can be expressed in a closed formula. If the effect represented by the R resistance is in a material section near to the junction and thermally strongly coupled to it, we can say

$$R_{the} = R_{thr} - h_O \frac{P_D}{P_D + P_R} R_{thr} = (1 - h_1) \cdot R_{thr} \qquad (12)$$

Equation (12) implies that with a “hot” resistor we experience expanding R_{the} curves at growing power levels. If the effect represented by P_R is in a material section far from the junction and well cooled, we get (for details see [6]):

$$R_{the} = R_{thr} - \left(h_O \frac{P_D}{P_D + P_R} + \frac{P_R}{P_D + P_R} \right) \cdot R_{thr} = \left(1 - h_1 - \frac{P_R}{P_D + P_R} \right) \cdot R_{thr} \qquad (13)$$

With this model we shall experience both shrinking and expanding R_{the} curves at changing power levels.

Measurements summarized in section 3 suggest that we can build a better model assuming constant h_{int} internal quantum efficiency and h_{ext} light extraction efficiency. The model reflects three domains (Figure 11), the electrical, the optical and the thermal one, and can be used in electro-thermal and board level thermal simulations.

The LED is powered with $P_{el}=P_R+P_D$ caused by current I in the electric domain. A part of the P_D electric energy is converted to photons and appears as P_{opt_int} in the optical domain of the device. The link between the electrical and optical part is quite simple, electrons belonging to $\eta_{int} \cdot I$ generate photons of $h \cdot \nu$ energy each. The internal light power is

$$P_{opt\_int}=[(h_{int} \cdot I)/q] \cdot h \cdot n$$

or

$$P_{opt\_int}= U_q \cdot I \,, \qquad U_q=h_{int} \cdot E_g /q \qquad (14)$$

where $E_g=h \cdot \nu$ means the band gap belonging to radiative recombination. U_q is a model parameter of voltage dimension and can be calculated from measured device efficiency and physical constants.

Most photons leave the device and can be treated as emitted P_{opt}, remaining photons will be absorbed in the chip and the package and their energy appears in the thermal domain as P_{loss}. With the above h_{ext} light extraction efficiency we can say that $P_{opt}=h_{ext} \cdot P_{opt\_int}$ and $P_{loss} = (1-h_{ext}) \cdot P_{opt\_int}$.

In the thermal domain all resistive and optical losses appear and add to the heating at different points of the equivalent thermal network.

In the simplest model all heating effects can be concentrated on a single location as in Figure 11. The junction point is obviously heated by $P_D – P_{opt\_int}$. In the figure we assumed a single entry point for P_R and P_{loss} , too.

<u>We can define *model level 2*</u> supposing constant h_{int} and small current level. Besides (14) we can state that $P_{heat}=P_D–P_{opt\_int}$ and introducing

$$h_2 = P_{opt\_int} / P_{el} = U_q \cdot I / P_D = U_q / U_D \qquad (15)$$

we get

$$R_{the} = R_{thr} \cdot P_{heat} / P_D = (1-h_2) \cdot R_{thr} \qquad (16)$$

<u>For *model level 3*</u> we add electric losses as $P_{el} = P_D+P_R$. Now we have

$$h_3 = P_{opt\_int} / P_{el} = U_q{}^{x} I / (P_D+P_R)= U_q / (U_D+U_R) \qquad (17)$$

R_{the} depends on the “cold” or “hot” position of the resistor again. Equations (5) and (6) are valid, replacing h_0 by h_2 and h_1 by h_3 in them. Refer to Table 2 of [7] for measured and calculated values of the above model parameters.

Comparing measured results to efficiency and thermal resistance curves of the different model levels we experienced that the assumptiom of constant quantum efficiency and a serial resistance in a „rather cold than hot” position (level 3) gives best approach.

4.2 Simulation of numerical models

Based on Figure 11 we also created a general LED macro model for a SPICE-like circuit simulator. The thermal sub-model was created by fitting the element values of the five ladder stages to the plateaus of the cumulative structure function of the investigated LED. The simplified circuit diagram of the LED circuit model is shown in Figure 12.

In our study we used an electro-thermal simulator which contains a dynamic diode model comprising the ideal characteristics and additional physical effects. Selecting proper device parameters we dulled the diode model to produce basic $U_D = mU_T \cdot \ln(I/I_0)$ characteristics, and diffusion and space charge capacitances only. Cross-effects were modeled by controlled sources, such as voltage controlled voltage source, voltage controlled current source (one of them is sufficient), and bilinear source producing a current proportional to two other voltages. The complete model became rather intricate, a fragment of it is shown in Figure 13. The picture shows how *currents* proportional to *power* are produced in a quasi-analog computational technique. IPloss and (IP_e_junct – IPopt) are computed in similar way. The thermal RC ladder delivers *voltages* proportional to *temperature*.

We simulated our model at the same current levels which were used in some of our measurements. The subsequent figures show the results of a simulation where the input current was switched from 400 mA to 10mA at the 5th nanosecond. Figure 14 shows all thermal node temperatures in the 100 ns to 300 s range. The dashed line represents the electric transient, i.e. the forward voltage scaled to temperature through the −1.84 mV/°C calibration factor. After a few μs this curve coincides with the node temperature at `junct`.

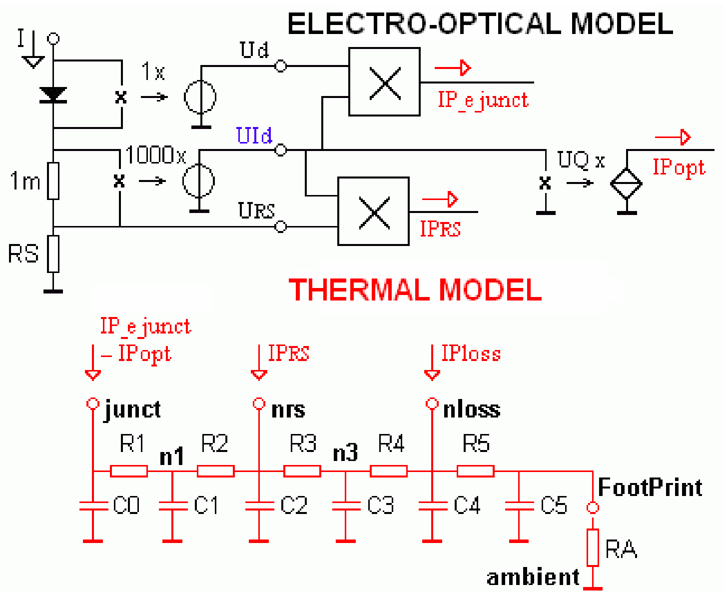

Figure 13: Circuit macro model of a LED aimed at SPICE-like simulations

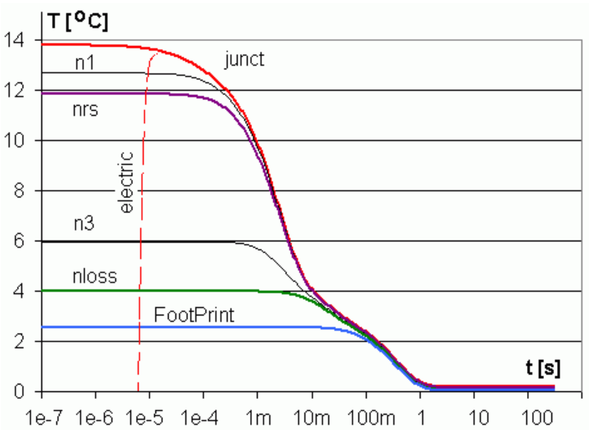

Figure 14 Transient results: node temperatures at 400 mA

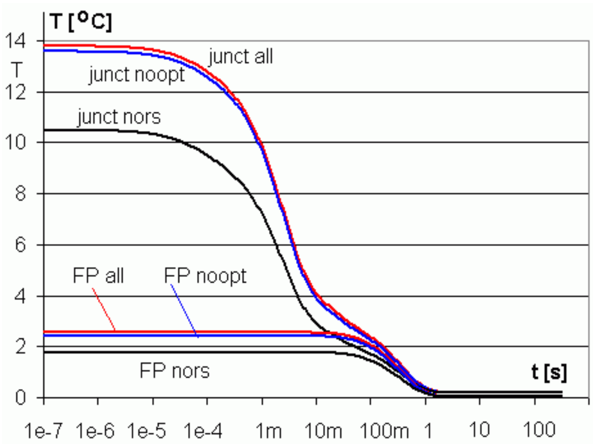

Figure 15 Junction and footprint temperatures at 400 mA: all effects, electrical or optical losses neglected

Figure 15 shows junction and footprint temperatures if electric or optical losses are neglected, i.e. respective currents do not flow into the `nrs` and `nloss` nodes.

In Figure 16 we compare measured and simulated results. We fit the curves at their hottest point – this is arbitrary because we presented temperature differences. The curves run parallel in most ranges. We see larger difference below 10 μs because of the initial electric transient; and after the 1 second magnitude. We have to note that after a few seconds the thermal wave propagates in the cooling fixture, which is modeled by a single resistance only. The model of the fixture could be improved by adding a few R and C components but this was not our target now. Figure 17 shows a comparison of differential structure functions. The curves s1, s2, s4, s8 were calculated from simulated cooling transients at 100 mA, 200 mA, 400 mA and 800 mA powering, respectively.

The facts that the transients in Figure 16 fit well and the peaks of s4 and m4 coincide in Figure 17 show that we extracted the model parameters correctly from the curves belonging to 400 mA. The real merit of the model is that it yields the footprint temperature transients and reflects the changes of R_{th} at different currents.

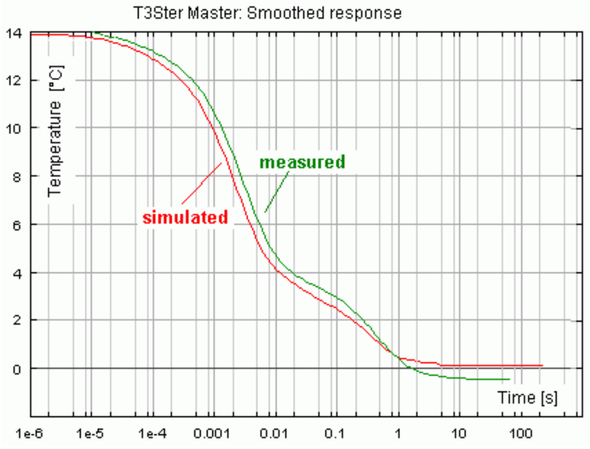

Figure 16: Comparison of measured and simulated transients at 400 mA powering

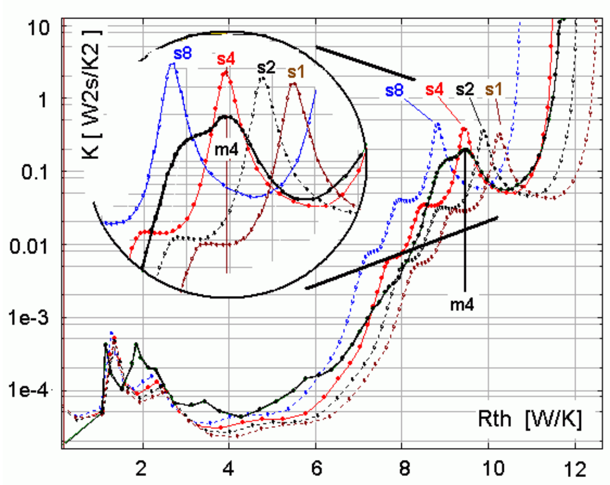

Figure 17: Differential structure functions derived from measured and simulated transients at different powering

5 Summary

With our measurements we found that the thermal behavior of LEDs depends on the applied power level. In order to obtain accurate thermal measurement results we propose combined thermal transient and photometric/radiometric measurements. We also propose using actively cooled test fixtures in these measurements

- for stabilizing temperature of LED samples (DUT) and standard LEDs during the optical measurement in the integrating sphere, in order to avoid thermal drifts such as shown in Figure 1
- as constant boundary (cold-plate) for the LED samples during the thermal transient measurements.

We realized that devices with parallel energy transport cannot be characterized by a single thermal resistance value: We have to make a distinction between the R_{the} *effective thermal resistance* describing the whole device and R_{thr} *real internal thermal resistance* describing the package. Based on our recent experience it seems, that in case of the characterization of power LEDs some standards of CIE and JEDEC need to be matched.

In order to better understand our measurement results we set up different analytical models for the efficiency and thermal resistance of power LEDs. Besides the analytical ones we created a numerical model too. It has been successfully implemented as circuit macro model to be used with an electro-thermal circuit simulation program. With this model we accurately described the electrical and the thermal behavior of power LEDs and reproduced the observed device behavior such as variation of structure functions with the applied power level.

6 Acknowledgement

This work was supported by the AGE 0045/03 TERALED project of the Hungarian Government. Many thanks are due to P. Szabó of MicReD, Gy. Bognár of BUTE and K. Seelin of Seelink Technologies for their contributions to our thermal transient measurements. We are grateful to S. Haque and Q. Van Voorst Vader of Lumileds for providing us Lumileds Luxeon LED samples.

7 References

[1] www.micred.com/t3ster.html

[2] http://www.jedec.org/download/search/jesd51-1.pdf

[3] V. Székely and Tran Van Bien: "Fine structure of heat flow path in semiconductor devices: a measurement and identification method", *Solid-State Electronics*, V.31, pp.1363-1368 (1988)

[4] V. Székely: "On the representation of infinite-length distributed RC one-ports", *IEEE Trans. on Circuits and Systems*, Vol.38. pp. 711-719 (1991)

[5] www.micred.com/strfunc.html

[6] G. Farkas, Q. van Voorst Vader, A. Poppe, Gy. Bognár: Thermal investigation of high power optical devices by transient testing, Proc. of the 9th THERMINIC, Aix-en-Provence, France, Sep 2003, pp 213-218

[7] G. Farkas, S. Haque, F. Wall, P. S. Martin, A. Poppe, Q. van Voorst Vader, Gy. Bognár: Electric and thermal transient effects in high power optical devices, The 20th IEEE SEMI-THERM Symposium, 9-11 March 2004, San Jose, CA, USA